Arch. Metall. Mater. **70** (2025), 2, 737-748

DOI: https://doi.org/10.24425/amm.2025.153476

Y. WU[1], Y. LIAO[1*], H. MA[1], J. LI[1]

BEHAVIOR AND STUDY OF THE KINETICS ASPECTS OF HYDROTHERMAL LEACHING CONDUCTED ON THERMAL ACTIVATED PRODUCTS OF COMPLEX POLYMETALLIC SECONDARY SULFIDE CONCENTRATE

The utilization of complex polymetallic secondary sulfide concentrate (CPSSC) is difficult, owing to its special structure and composition. In this paper, CPSSC was firstly activated by roasting under atmosphere, followed by hydrothermal leaching under oxygen pressure with water. The mineral phase structure and morphology of the activated products and leached residues were characterized by XRD and SEM-EDS to study the leaching behavior and kinetic characteristics of copper from CPSSC. The obtained results show that the optimum conditions for hydrothermal leaching of the roasting activated products of CPSSC under oxygen pressure with water are as follows: leaching temperatures 185°C, oxygen partial pressure 0.6 MPa, liquid solid ratio 12.5:1, stirring rate 600 r/min. Under the above conditions, the iron and lead existing in the activated products were mostly transferred and remained in leached residue with the state of iron oxide and lead sulfate respectively, and the leaching rate of Cu reached 95.73%. The kinetic analysis show that the extracting of copper from the activated product by hydrothermal leaching under oxygen pressure obeys chemical reaction control model, with activation energy calculated as 41.98 kJ/mol by Arrhenius equation, and the leching kinetic equation of copper could be expressed as: $1-(1-X)^{\frac{1}{3}} = 0.437 P_{O_2}^{1.258} w^{0.728} e^{\frac{-5049.7}{T}} t$.

Keywords: Chalcopyrite; thermal activation; hydrometallurgy; kinetics

1. Introduction

Chalcopyrite is one of the major copper minerals, accounting for more than 70 wt.% of global copper reserves, and is also widely distributed in solid waste and secondary resources containing copper [1-4]. The extraction of copper from chalcopyrite can be implemented by pyrometallurgical and hydrometallurgical processes [5,6]. However, the emission of polluting gases and toxic compounds, such as SO_2, CO_2, NO_x etc. from the pyrometallurgical process causes a major threat to the aquatic environment and atmospheric environment, resulting in increased energy consumption and costs [7-9]. Alternatively, the hydrometallurgical process has environmental and economic advantages, and it is gradually replacing the traditional pyrometallurgical process and becoming the primary choice for treating chalcopyrite, especially complex polymetallic secondary chalcopyrite concentrate (CPSSC) which is easily found with the overexploitation of copper mine. Therefore, the methods separating valuable metals from CPSSC by hydrometallurgical process have been extensively studied, such as bioleaching with the result that high copper extraction rate was obtained when the solution potential was controlled within a suitable range [10], atmospheric pressure oxidation leaching which needs consuming a lot of oxidants [11-14], ionic liquid leaching which demonstrated ionic liquid based lixiviants with more polar cations appear to show better extraction than those with less polar cations [15], ammonia leaching which testified a flat passivation layer of FeOOH was formed resulting from the selectively leaching of Fe prior to Cu [16], and pressurized acid leaching which demonstrated that temperature had the greatest influence on copper extraction and the kinetics for the leaching copper from chalcopyrite was controlled by chemical reaction equation [17]. However, as the reason that chalcopyrite, the main constituent in CPSSC, has a crystal structure with tetrahedral coordination by copper, iron and sulfur [6,18], each sulfur ion located at a tetrahedral angle is surrounded by four ions of copper and iron. Furthermore, copper and iron are located in the same lattice, resulting the leaching of iron in large quantities along with copper during leaching

[1] KUNMING UNIVERSITY OF SCIENCE AND TECHNOLOGY, FACULTY OF METALLURGICAL AND ENERGY ENGINEERING, KUNMING 650093, CHINA

* Corresponding author: liaoylsy@163.com

process, increasing the difficulty in further process for removing iron from the leaching solution obtained. In addition, passivation layer formed on its surface during the leaching of chalcopyrite restricts the contact and diffusion process between leaching agent and minerals, which is nominated as passivation effects, leading to low leaching rate of valuable metals from chalcopyrite [1,6].

To improve the leaching rate and final recovery of valuable metals from chalcopyrite, numerous studies have been carried out. The process of hydrothermal leaching without acid under oxygen pressure atmospheric, which can achieve high extractive leaching rate of copper and zinc from CPSSC [19]. However, it needed to be conducted under a higher temperature at 200°C, resulting a harsh requirement for leaching instruments. In recent years, researchers have found that the leaching rate of copper from chalcopyrite can be improved by pretreatment enhancements before leaching, such as mechanical enhancement, microwave enhancement, ultrasonic enhancement, and etc. Mechanical enhancement can distort the crystal lattice and increase the specific surface area of minerals, resulting in the conversion of some mechanical energy into internal energy of the material and accelerating leaching reaction rate [20]. Microwave enhancement can reduce the passivation effect in leaching process, improve the oxidation leaching performance of chalcopyrite and increase the leaching rate of valuable metals [21]. Ultrasonic enhancement increases the diffusion inside the mineral particles, removes the passivation layer formed by element sulfur, and increases the chemical reaction to dissolve more chalcopyrite [22]. However, the mechanical enhancement is energy-intensive and high requirement for equipment, and the effecting mechanism of microwave and ultrasonic on the recovery of valuable metals is still vague and controversial [23,24], limiting its further development. Thermal activation pretreatment can not only solve the co-leaching of copper and iron, realize the selective extraction of copper, improve the leaching conditions of valuable metals from chalcopyrite ore, but also distort the lattice structure and improve the leaching rate of valuable metals.

In this work, the effect of thermal activation pretreatment on copper leaching rate from CPSSC was studied by thermal activation of CPSSC then followed by oxygen pressure leaching without acid. On this basis, the changes in surface chemical forms and morphology of CPSSC and leached residue after activation were investigated by X-ray diffraction (XRD) and scanning electron microscopy (SEM) characterization methods. As the reason that zinc is easier leached than copper, the optimum leaching conditions were defined to achieve almost complete leaching of copper from CPSSC, and the leaching behavior and reaction kinetics of copper from the activated products of CPSSC by hydrothermal leaching under oxygen pressure condition with water were investigated.

2. Experimental

2.1. Materials

The raw material used in the experiments, a typical CPSSC with high lead and iron content and low copper content, came from a concentrator in Yunnan. Its chemical composition was shown in TABLE 1. The reagents (sulfuric acid, sodium lignosulfonate, sodium thiosulfate, potassium iodide, etc.) used in the experiments were analytical pure, and deionized water was manufactured in ourself laboratory.

2.2. Experimental method

30.0 g CPSSC with particle size of -75 μm was activated by roasting under atmosphere at 350°C for 2 h in tubular furnace, then cooled in the furnace to ambient temperature for getting activated products (also named as pyrolysis products). Subsequently, the activated products were leached in an autoclave (YZUR-500, Shanghai Yanzheng Experimental Instrument Co. Ltd, China) at conditions of pressured oxygen atmosphere with water. Which the activated products were mixed with distilled water according to a specified liquid-solid ratio and added into the autoclave, followed by heating to the specified temperature, then highly purified oxygen was injected to maintain the required oxygen partial pressure to react for 4 h. Samples were taken with 15 min interval in the first two hours and with 30 min interval in the last two hours during leaching process. In the end, the autoclave was cooled in the air, and the obtained pulp was removed and filtered to get the leachate and leached residue.

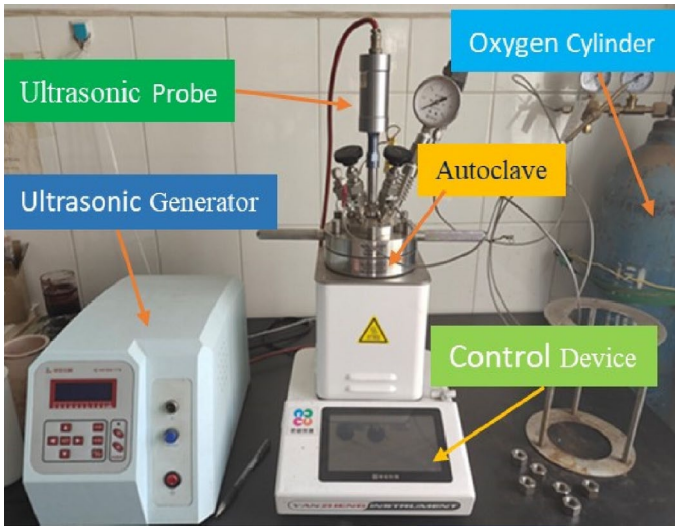

Fig. 1. Picture of the experimental apparatus for leaching process

TABLE 1

Chemical composition of the main elements of the raw material

Element	Cu	Fe	S	Zn	Pb	SiO_2	MgO	CaO	Al_2O_3	Others
Contents/ wt.%	11.10	28.10	34.95	2.97	8.88	1.86	0.43	0.38	0.50	10.83

The leached residue was dried in oven at 105℃ for 2 h prior to further be analyzed.

The picture of the experimental apparatus for leaching process was shown in Fig. 1.

2.3. Analysis and characterization methods

Quantitative determination of chemical elemental content in the raw material, pyrolysis products, and leached residues were conducted by inductively coupled plasma atomic emission spectrometer (ICP-AES, Optima-5300DV, Pekin-Elmer, USA). X-ray diffractometer (XRD, X' Pert Pro MPD, PanacoAnalytical Instruments, Netherlands) was used for mineral phase characterization with Cu-Ka target (λ = 0.15406 nm) as the radiation source, under the conditions of tube voltage of 40 kV, tube current of 40 mA, scanning speed of 10°/min, and scanning interval of 5°~90°. The JSM-6360 scanning electron microscope (SEM) with elemental mapping was used to analyze the morphology of the raw material, the pyrolysis products, and the leached residues. The sulfur content was determined using a carbon and sulfur analyzer (ELTRA CS2000, Eltek, Germany). The copper contained in the leachate was detected by iodimetry [25] and the copper leaching rate was calculated by Eq. (1).

$$X_i = \frac{\left[v_0 - \sum_{i=1}^{i-1} V_i\right] \times C_i + \sum_{i=1}^{i-1} V_i \times C_i}{100 \times w} \quad (1)$$

where X_i is the i-th leaching rate of copper, %; V_0 is the total volume of leachate, L; V_i is the volume of liquid sample taken out at every i-th interval, L; C_i is the concentration of copper in the liquid samples taken out at the i-th time, g/L; w is the mass fraction of elements in the raw material, %.

3. Results and discussion

3.1. Characterization of mineral phase structure

The characterization results of XRD analysis of raw material and pyrolysis products were shown in Fig. 2, from which it can be seen that CPSSC and the products pyrolyzed at 350℃ are mainly composed of chalcopyrite ($CuFeS_2$), PbS (galena), FeS_2 (pyrite) and ZnS (sphalerite). The diffraction peaks of $PbSO_4$ appear obviously in the products pyrolyzed at 350℃, indicating that part of the mineral phase of galena in CPSSC was dissociated to form $PbSO_4$ while CPSSC was activated at this temperature. The reason why not pyrolyzing at higher temperature than 350℃ is that hazardous gas SO_2 will emit resulting from the decomposition of metal sulfides in air atmosphere, and on the contrary the leaching efficiency of valuable metals is not ideal while the pyrolyzed products at temperature blower than 350℃ used for leaching.

The SEM-Mapping spectra of the raw material and the pyrolysis product were respectively show in Figs. 3 and 4.

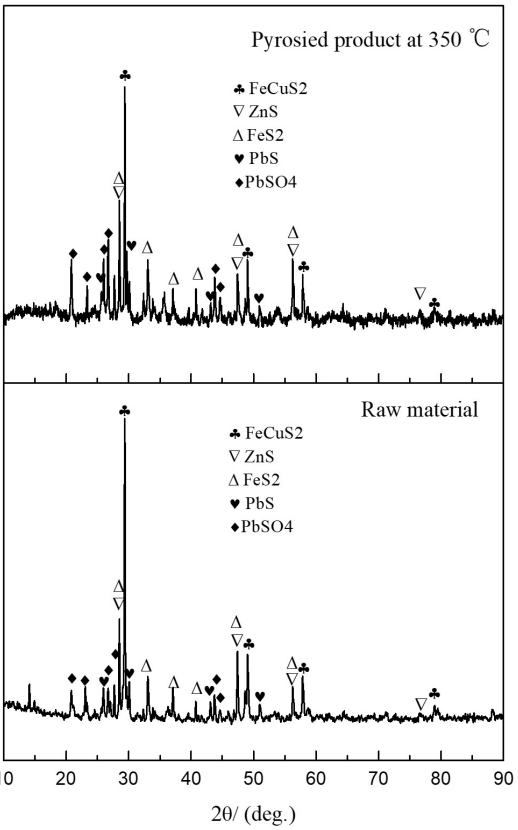

Fig. 2. XRD patterns of raw materials and pyrolysis products

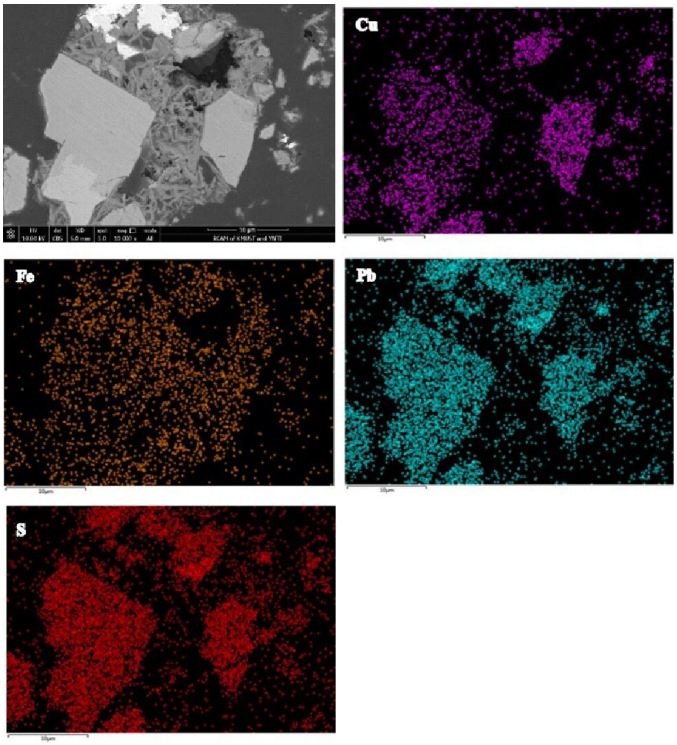

Fig. 3. SEM-Mapping spectrum of raw materials

It can be observed from Fig. 3 that the various sulfide mineral phases composing the raw material are intergraded with each other, and especially that Cu, Fe and S are located at the same area. And it is also found from Fig. 4 that loose structure ap-

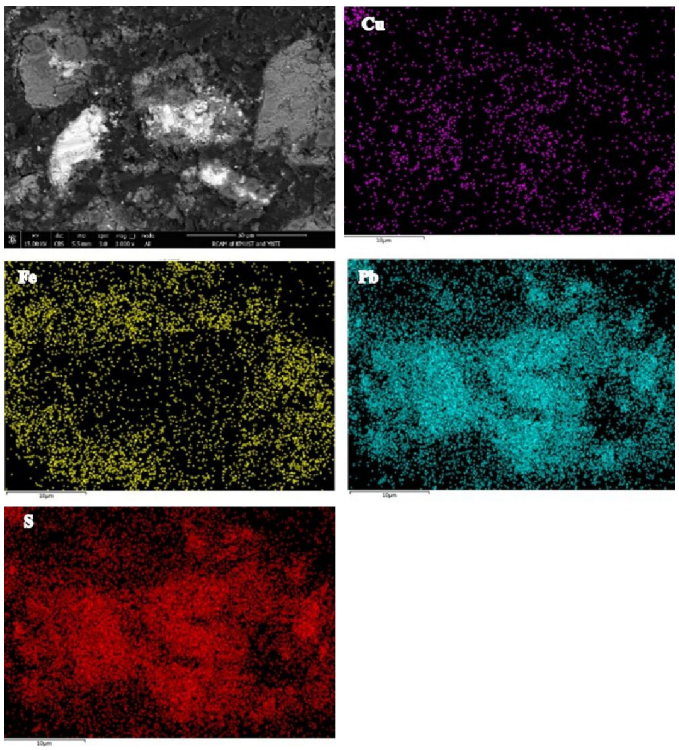

Fig. 4. SEM-Mapping spectrum and surface scan of pyrolysis product thermal activated at 350°C

pears in the pyrolysis products, which plays an important role in increasing the specific surface area and self-corrosive current [26]. Moreover, the results of elemental mapping in Fig. 4 show that, compared with the raw material, Cu and Fe elements are distributed scattered while Pb and S are more concentrated together in pyrolysis product.

3.2. Effect of factors on Cu leaching rate

3.2.1. Effect of leaching temperature

The effect of leaching temperature on the pressurized leaching copper from pyrolysis product was investigated. The effect of leaching temperature on the leaching rate of Cu under the conditions of oxygen partial pressure of 0.8 MPa, liquid to solid ratio of 12.5:1, stirring rate of 600 r/min, and dosage of sodium lignosulfonate of 0.5% mass pyrolysis product was shown in Fig. 5(a). As shown in the figure that Cu leaching rate increased from 59.51% to 95.73% when the temperature was increased from 155°C to 185°C. This result is consistent with the conclusion achieved by Berry et al [27], who found that the reaction rate doubled whenever the temperature was increased by 10°C. When the temperature was at 185°C, the reaction was more intense and the growth of Cu leaching rate was faster after the reaction time exceeds 120 min. Whereas, on the conditions of other temperatures, for getting the same trend it needed 135 min. The XRD patterns of leaching residues obtained at temperature 155°C and 185°C were illustrated in Fig. 5(b), from which it can be seen that the mineral phases in the leached residue at the leaching temperature of 155°C are FeS_2, Fe_2O_3, $CuFeS_2$, and $PbSO_4$, indicating the leaching of pyrolysis product is not completely. However, the minerals phases of the leached residue at the leaching temperature of 185°C are mostly iron oxide and lead sulfate and few chalcopyrite can be found, meaning the obtained residue easy to further be utilized and the leaching of pyrolysis product completely. This leads to the result that the leching temperature of 185°C was more suitable.

The characterization results of leached residues by SEM-Mapping at leaching temperatures of 185°C and 155°C were shown in Fig. 6 and Fig. 7 respectively. It can be discovered by SEM in Fig. 6 that the morphology of leached residue obtained at 185°C has a loosen structures scatted with squared well-crystal block which is aggregated area of Pd, S and O, meaning the composition of lead sulfate, and the other area is central area of Fe and O which is in consistent with the composition of Fe_2O_3. By observing the imagines (Fig. 7) tested by SEM of the leached residue at 155°C, it can be obtained that the morphology of the leached residue is granulated scatted with little particles where mainly compose of CuS besides $PbSO_4$ and Fe_2O_3, which is tested by mapping analysis.

3.2.2. Effect of oxygen partial pressure

Base on experiment 3.2.1 mentioned above, the effect of oxygen partial pressure on the pressurized leaching of pyrolysis

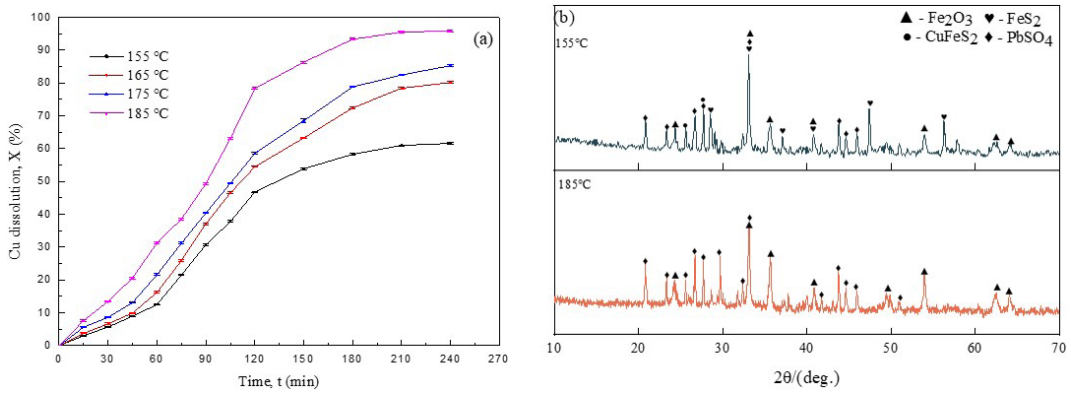

Fig. 5. (a) Effect of leaching temperature on Cu leaching rate; (b) XRD patterns of leached residue at leaching temperature of 185°C and 155°C

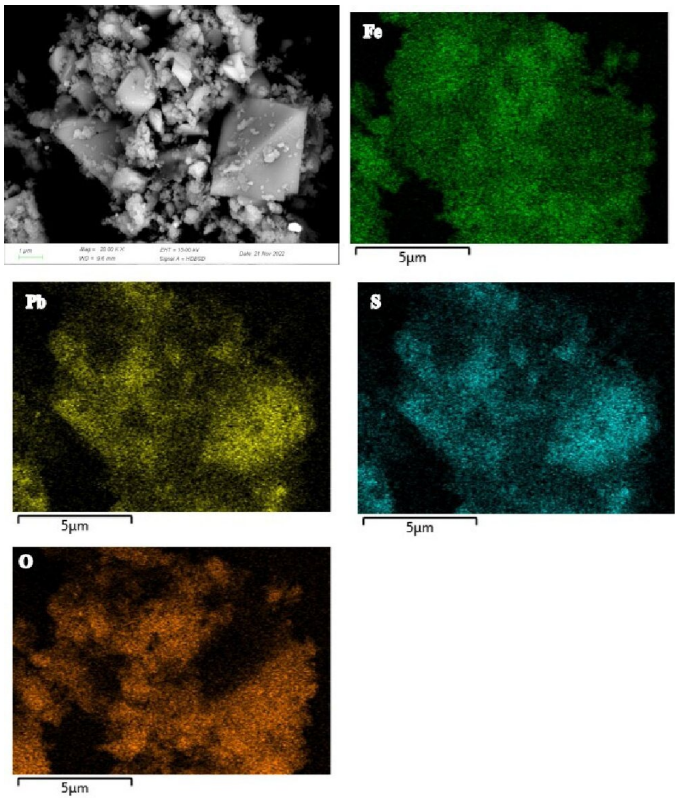

Fig. 6. SEM-Mapping patterns of leached residue at 185℃

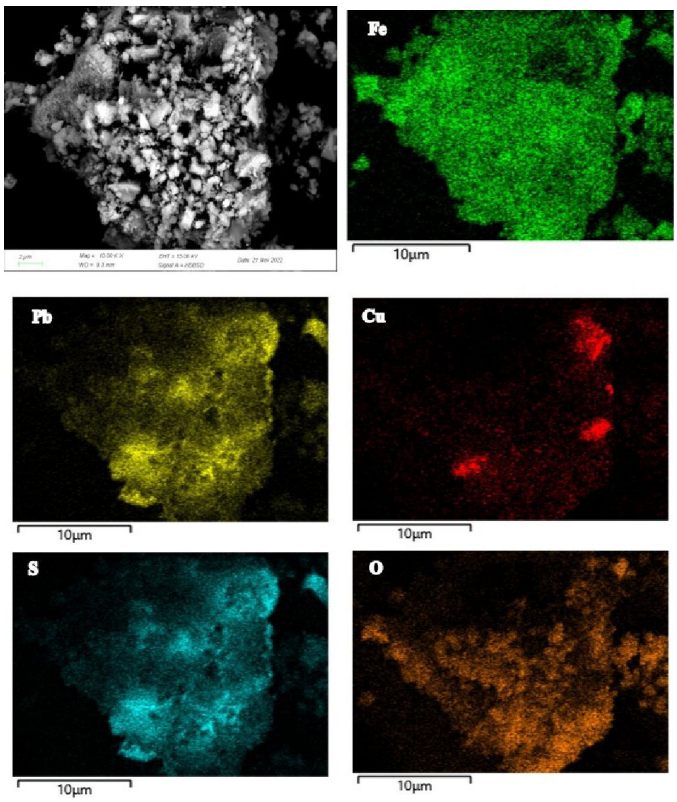

Fig. 7. SEM-Mapping patterns of leached residue at 155℃

product was investigated at leaching temperature of 185℃, liquid to solid ratio of 12.5:1, stirring rate of 600 r/min and sodium lignosulfonate dosage of 0.5% mass present of pyrolysis product. The effect of oxygen partial pressure on the leaching rate of Cu was shown in Fig. 8. As shown in the figure, the highest dissolution rate of Cu was achieved when the oxygen partial pressure was increased to 0.8 MPa, and the maximum dissolutions of Cu reached 95.73%. The increase in oxygen partial pressure leads to an increase in the total pressure of the autoclave, which can lead to the formation of iron oxide compounds based on the oxidation of sulfates in pyrolysis product. The XRD analysis (Fig. 8b) shows that the material phase of leached residue obtained at oxygen partial pressure 0.4 MPa are mostly iron compounds and lead sulfate, as well as also a small amount of pyrite, which investigates the dissolution of raw material is not completely. By observing the SEM-Mapping patterns of the leached residue obtained at 0.4 MPa (Fig. 9), it can be found that the surface morphology is loose, mostly small particles accompanied by lump, and that S, Pb and O are located in the same area and Fe mainly exists with O in the same district, meaning the main chemical composition of the residue consist of $PbSO_4$ and Fe_2O_3.

Combined with the results from the influence on leaching rate and characterization of XRD and SEM-Mapping on the leached residues, the leaching conditions at an oxygen partial pressure of 0.8 MPa are better to obtain the target substances. Therefore, 0.8 MPa should be selected as the optimal oxygen partial pressure under these circumstances for the next study.

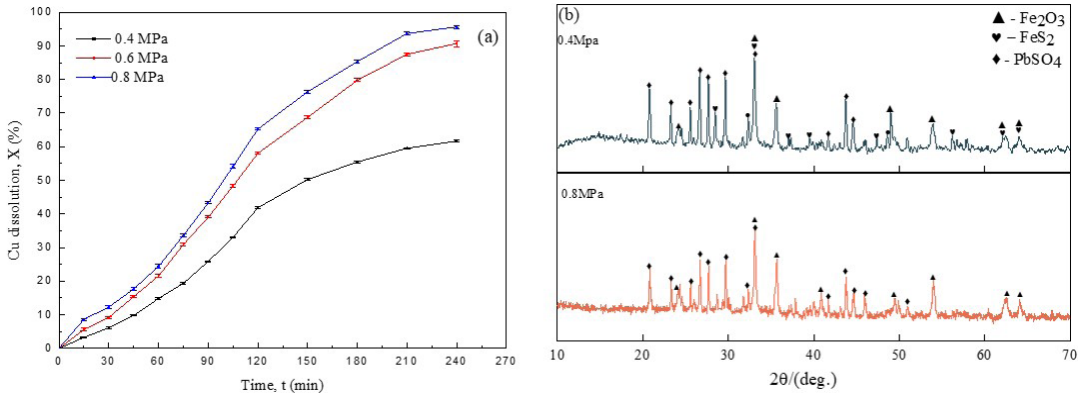

Fig. 8. Effect of oxygen partial pressure on Cu leaching rate(a) and XRD patterns of leached residue at oxygen partial pressure of 0.4 MPa and 0.8 MPa (b)

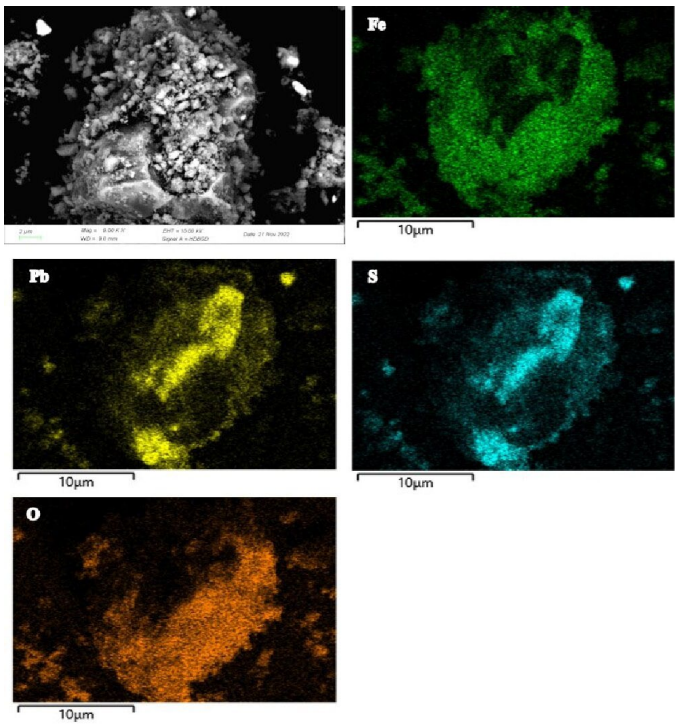

Fig. 9. SEM-Mapping pattern of leached residue with oxygen partial pressure of 0.4 MPa

3.2.3. Effect of liquid to solid ratio

On the basis of the above experiments, the effect of liquid to solid ratio on the pressurized leaching of pyrolysis product was investigated at liquid to solid ratios of 10:1, 12.5:1 and 15:1, respectively. The effect of liquid to solid ratio on the Cu leaching rate at leaching temperature of 185℃, partial pressure of oxygen of 0.8 MPa, stirring rate of 600 r/min and sodium lignosulfonate dosage of 0.5% mass present of pyrolysis product was shown in Fig. 10(a).

From Fig. 10(a), it can be seen that the trends of leaching rate of Cu are approximately the same and the final leaching rates are similar under these three conditions. As shown by XRD of leaching slag with different liquid to solid ratios in Fig. 10(b), the main components of leached residue in all three conditions are compounds of Fe and Pb, but at a liquid to solid ratio of 10:1, the residue also contains small amounts of Cu and Fe compounds. And when the liquid to solid ratio exceeds 12.5:1, the main components of the residue are the oxide of Fe and the compound of $PbSO_4$. As the reason that high ratio of liquid to solid will cause waste of water resources and leads big volume of leaching instruments, it is more appropriate that the ratio of liquid to solid 12.5:1 is selected.

3.2.4. Effect of stirring rate

The effect of stirring rate on Cu leaching rate was investigated at stirring rates of 400, 500 and 600 r/min, respectively, on the conditions of leaching temperature of 185℃, oxygen partial pressure of 0.8 MPa, liquid to solid ratio of 12.5:1, and sodium lignosulfonate dosage of 0.5% mass present of pyrolysis product, the results obtained were showed in Fig. 11(a). From which it can be found the copper leaching rate increased from 85.32% to 95.73% when the stirring rate was increased from 400 to 600 r/min. This can be accounted by the reason that high stirring rate causes better contact between pyrolysis product and leaching reagent and improved the leaching rate, meaning a significant effect on the copper leaching rate. Additionally, high stirring rate enhances the diffusion of the leaching reagent to the outer surface of the solid particles and reduces the thickness of the diffusion layer formed around the particles [28]. When the stirring rate was 600 r/min, the leaching rate of Cu is maximum, which means that the stirring rate of 600 r/min is the most effective rate for gas-liquid-solid transfer in reaction system [29].

In addition, the XRD patterns of the leached residue with stirring rates of 400 r/min and 600 r/min were shown in Fig. 11(b) respectively. The XRD analysis (Fig. 11(b)) shows that the leached residue is mainly lead sulfate and pyrite at the stirring rate of 400 r/min. For further investigating the mineral phase in

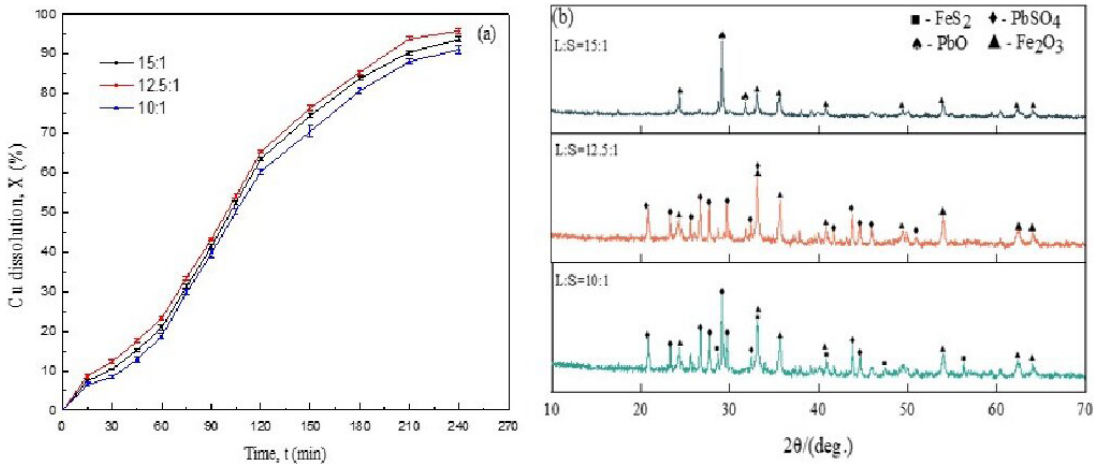

Fig. 10. (a) Effect of liquid to solid ratio on Cu leaching rate; (b) XRD of leached residue with liquid-to-solid ratios of 10:1, 12.5:1 and 15:1, respectively

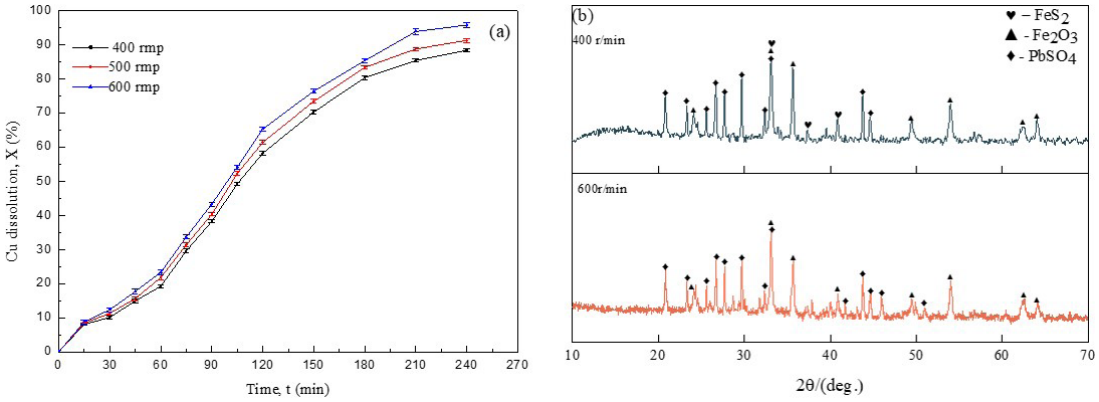

Fig. 11. (a) Effect of stirring rate on the leaching rate of Cu; (b) XRD patterns of leached residue with stirring rates of 400 r/min and 600 r/min, respectively

the leached residue, the SEM-Mapping of the leached slag at 600 r/min were performed and the results were shown in Fig. 12. It can be observed from Figure 12 that the leached residue has the structure of loosen particles embedded lumpy, and that S, Pd and O are distributed in the same area, as well as Fe exists with O. Additionally, it is demonstrated from Fig. 11(b) that the composition of leached residue with stirring rate of 400 r/min is more complicated as the reason that the existing of FeS_2, which increases the subsequent lead-iron separation work. Therefore, 600 r/min is chosen as the optimum stirring rate.

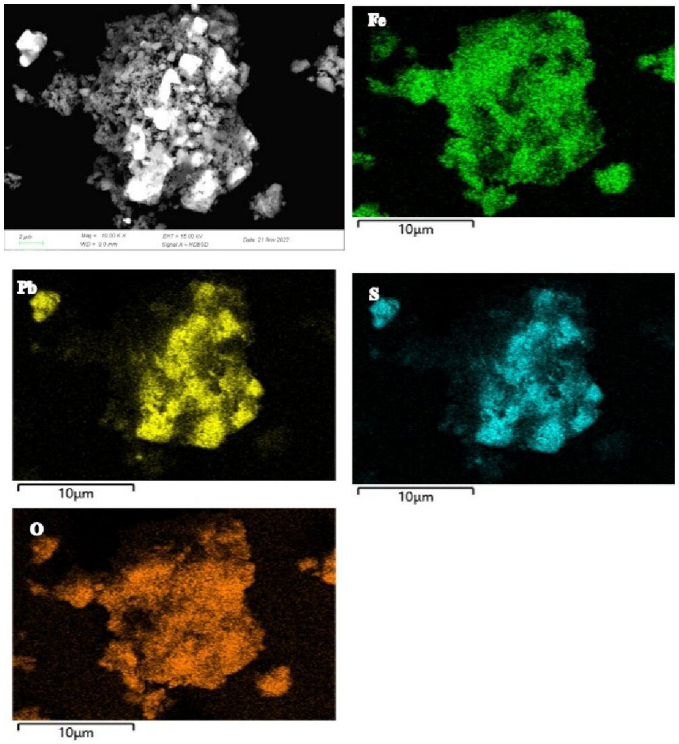

Fig. 12. SEM-Mapping patterns of leached residue with stirring rate of 400 r/min

3.3. Thermodynamically feasible and spontaneous

It is important to indicate the chemical reaction of the realized leaching, which refers to the calculation of the activation energy, and it is also necessary to calculate the probability of its progress (delta G). In the conditions for leaching valuable metals from CPSSC, the main chemical reactions and their standard Gibbs energy were calculated and listed in TABLE 2 based on the thermodynamic data in literature [30]. From the value of the standard Gibbs energy in TABLE 2, it suggests that chemical reactions of the realized leaching are thermodynamically feasible and spontaneous as the reason that the standard Gibbs energy of these reactions during leaching is minus. Although it is known that chalcopyrite is dissolve in acidic leaching medium, why can water be used as leaching agent in the present work! This because that FeS_2 contained in the CPSSC reacted with water and oxygen to produce sulfuric acid needed to dissolve chalcopyrite, and the concentration of sulfuric acid is about 15-25 g/L in the leachate, as the results of pH of leachate is 0.81-0.59.

TABLE 2

The standard Gibbs energy (kJ/mol) of the main chemical reactions in leaching

No.	Chemical reaction	$\Delta_r G^\theta_{298K}$	$\Delta_r G^\theta_{428K}$	$\Delta_r G^\theta_{438K}$	$\Delta_r G^\theta_{448K}$	$\Delta_r G^\theta_{458K}$
1	$2FeS_2\,(s) + 7O_2\,(g) + 2H_2O\,(aq) = 2Fe^{2+}\,(aq) + 4H^+\,(aq) + 4SO_4^{2-}\,(aq)$	–559.887	–498.098	–489.52	–484.409	–476.854
2	$4FeS_2\,(s) + 15O_2(g) + 2H_2O\,(aq) = 4Fe^{3+}\,(aq) + 4H^+\,(aq) + 8SO_4^{2-}\,(aq)$	–1162.16	–1015.37	–995.73	–983.361	–965.94
3	$FeCuS_2\,(s) + 4H^+\,(aq) + O_2(g) = Cu^{2+}\,(aq) + Fe^{2}\,(aq)^+ + 2S^0\,(s) + 2H_2O\,(aq)$	–80.899	–65.077	–63.236	–61.886	–59.874
4	$2ZnS\,(s) + 4H^+\,(aq) + O_2(g) = 2Zn^{2+}\,(aq) + 2S^0\,(s) + 2H_2O\,(aq)$	–87.935	–77.202	–76.018	–75.335	–73.608
5	$2FeS_2\,(s) + 4H^+\,(aq) + O_2(g) = 2Fe^{2+}\,(aq) + 4S^0(s) + 2H_2O\,(aq)$	–74.513	–63.474	–62.584	–61.775	–60.538
6	$2PbS\,(s) + 4H^+\,(aq) + 2SO_4^{2-}\,(aq) + O_2(g) = 2PbSO_4\,(s) + 2S^0\,(s) + 2H_2O\,(aq)$	–99.773	–104.022	–104.86	–105.787	–106.076
7	$S^0\,(s) + 2H_2O\,(aq) + 3O_2\,(g) = 4H^+\,(aq) + 2SO_4^{2-}\,(aq)$	–288.792	–282.846	–281.978	–280.965	–280.182

3.4. Copper leaching kinetic studies

In order to determine the leaching mechanism of pyrolysis product under oxygen pressure conditions, the experimental data were analyzed using shrinkage core model. The shrinkage core model assumes that for dense solid reactants, the chemical reaction proceeds from external and internal, the solid and liquid reaction occurs at the surface of the solid material, where the solid reactants are initially surrounded by a fluid layer, mass transfer occurs between the solid and the liquid, with more and more solid products are produced, and the solid reactants gradually decrease until disappear. As the reaction proceeds, the unreacted solid core shrinks to the center of the solid, forming a porous products layer around the unreacted core. The kinetic model predicts the mechanism of the leaching copper from CPSSC where the chemical reaction which labelled as No. 2 in TABLE 2 takes place when chemical reaction control, diffusion control, or a mixed control model containing both diffusion and chemical reaction occurs [31,32].

If the reactions rate is controlled by the chemical reaction, the formula of integral rate for the reaction is expressed as Eq. (2).

$$1-\left(1-X\right)^{\frac{1}{3}}=K_r t \tag{2}$$

If the reactions rate is controlled by the diffusion through the product layer, the formula of integral rate for the reaction is expressed as Eq. (3).

$$1-\frac{2}{3}X-\left(1-X\right)^{\frac{2}{3}}=K_d t \tag{3}$$

And if the reactions rate is controlled by both the chemical reaction and the product layer, nominated as mixing control, the formula of integral rate for the reaction is expressed as Eq. (4).

$$1-\left(1-X\right)^{\frac{1}{3}}-\frac{1}{3}\ln\left(1-X\right)=K_m t \tag{4}$$

Where X is the chemical reaction fraction, %; K_r, K_d and K_m are the kinetic constants controlled by chemical reaction, diffusion through the product layer, and mixture of them; t is the reaction time.

In addition, the activation energy can be calculated according to Arrhenius equation (Eq. (6)) by making a graph with ln$K$ versus 1/T.

$$K=A\exp\left(-\frac{E_\alpha}{RT}\right) \tag{5}$$

where, K is the rate constant; A is the pre-exponential factor; E_α is the activation energy, kJ/mol; R is the gas constant, 8.314 J/K· mol; and T is the absolute temperature, K.

Logarithm is taken on the both sides of Eq. (5), then Eq. (6) can be obtained.

$$\ln K=-\frac{E_\alpha}{RT}+\ln A \tag{6}$$

Arrhenius plots can be got by plotting with ln$K$ versus against 1/T, and E_α and A can be calculated from the slope and intercept of the fitted equations. The experimental data in Fig. 5 were substituted into Eqs. (2) to (4) to make plot and fitted, and the results of the fitting are shown in Fig. 13. The parameters of

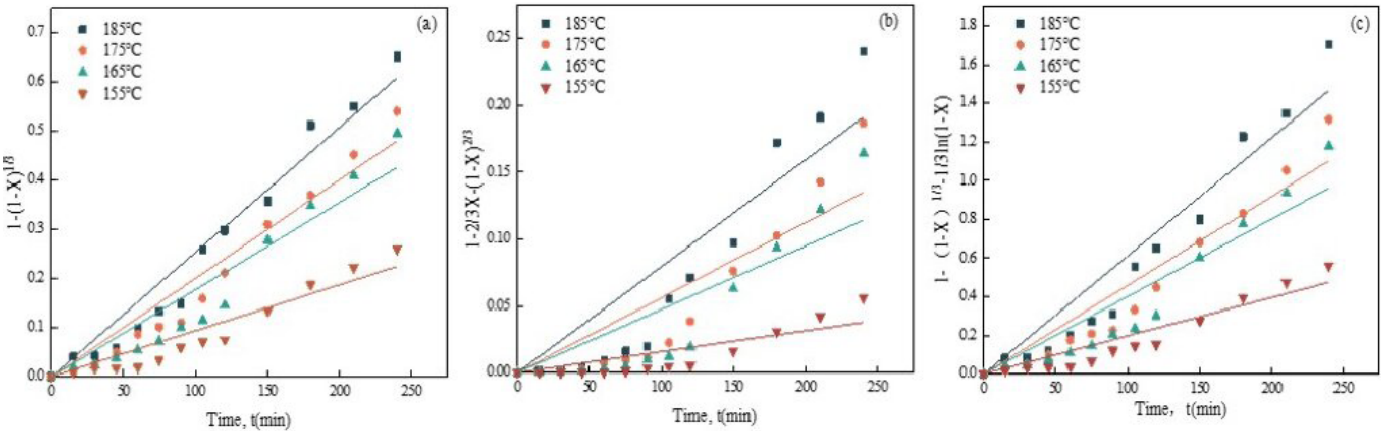

Fig. 13. Fitting curves for the variation of kinetic functions at different reaction temperatures (a: $1-1(1-X)^{1/3}$; b: $1-2/3X-(1-X)^{2/3}$; c: $1-(1-X)^{1/3}-1/3\ln(1-X)$)

TABLE 3

Parameters of control model at different reaction temperatures

Reaction temparature	Chemical reaction control		Internal diffusion control		Mixing control	
	K_r	R^2	K_d	R^2	K_m	R^2
185°C	2.530×10^{-3}	0.983	7.961×10^{-4}	0.905	6.110×10^{-3}	0.967
175°C	2.000×10^{-3}	0.976	5.619×10^{-4}	0.868	4.590×10^{-3}	0.961
165°C	1.770×10^{-3}	0.955	4.751×10^{-4}	0.830	4.010×10^{-3}	0.940
155°C	9.360×10^{-4}	0.953	1.570×10^{-4}	0.808	1.980×10^{-3}	0.947

its chemical reaction control model, internal diffusion control model and mixing control model are shown in TABLE 3.

Compared to the correlation coefficients controlled by internal diffusion reaction and mixing control, the results show that the correlation coefficient (R^2) values controlled by chemical reaction are closer to 1. Therefore, the kinetics leaching copper from CPSSC is consistent with chemical reaction control model. The results of the activation energy (E_α) calculated according to Arrhenius plots (Fig. 14) is 41.98 kJ/mol. It means that the reaction is controlled by the diffusion through the solid product layer when $E_\alpha < 12.55$ kJ/mol, and the reaction is controlled by the chemical reaction while $E_\alpha > 41.8$ kJ/mol [33,34]. The calculated value of activation energy is bigger than 41.8 kJ/mol, so the leaching of copper from CPSSC at different leaching temperatures is controlled by the chemical reaction model. The activation energy obtained in the present work is lower than that of 50.646 kJ/mol achieved by Ji et al. [35] while direct leaching copper from CPSSC with oxygen pressure leaching. The activation energy of the reaction can characterize the ease degree of reaction, indicating that the minerals is easily to be decomposed while it is activated, which facilitates further separation and extraction. When CPSSC is activated by thermal pyrolysis, the external energy is transferred to the chalcopyrite particles, causing the atomic arrangement of chalcopyrite to disordered and loose from regular and tight. As a result, the crystal structure of chalcopyrite is broken and the micro-strain such as defects in it is increased, the lattice size is become smaller and separated by high-energy grain boundaries, as well as the degree of amorphization is improved, leading to a decrease in the thermodynamic stability of the mineral [36,37] and the decrease in apparent activation energy while the pyrolysis product is leached [38].

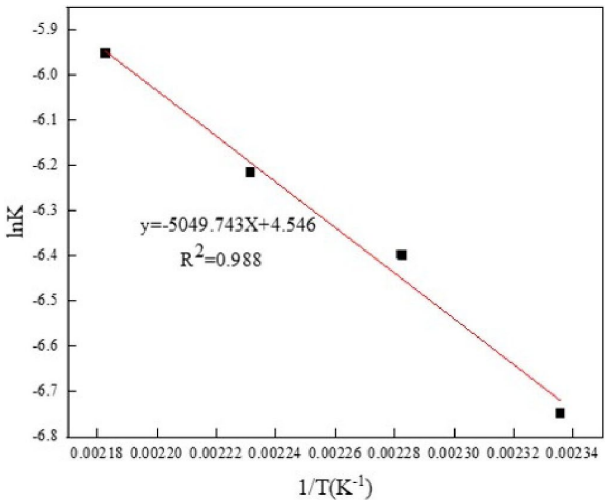

Fig. 14. Arrhenius plots of Cu leaching at different temperatures

Considering the influence of various factors on copper leaching rate, the relationship between the rate constant controlled by chemical reaction and various factors can be expressed as Eq. (7) [39,40]. The reason that stirring rate is considered is because it can affect the concentration of sulfuric acid produced from the reaction of FeS_2 with H_2O under oxygen pressured atmosphere [35], which also testified the results of the copper leaching rate nearly controlled by mixing control with a R^2 closed to 0.95 in TABLE 2.

$$1-(1-X)^{\frac{1}{3}} = K_0 P_{O_2}^{n_1} W^{n_2} e^{-\frac{E_\alpha}{RT}} t \quad (7)$$

where n_1 and n_2 are parameters of partial pressure of oxygen (MPa) and stirring rate (W), and K_0 is rate constant related to temperature; E_α is the apparent activation energy (kJ/mol); R is the gas equilibrium constant, 8.314 J/mol; T is the absolute temperature (K).

The effects of oxygen partial pressure (P_{O_2}) and stirring rate (W) on the leaching copper from CPSSC were applied to study the kinetic model, the obtained results can be found in Fig. 15 and Fig. 16 respectively. TABLES 4 and 5 show the reaction rate constants and correlation coefficients of the chemical control model, internal diffusion control model and mixing control model under different oxygen partial pressure and stirring rate conditions, respectively. From the table, it can be seen that under different oxygen partial pressure and stirring rate conditions, the chalcopyrite oxygen pressure leaching reaction are mainly controlled by the chemical reaction. The relationship graphs of $\ln K_r$ versus $\ln P(O_2)$ and $\ln w$ calculated from K_r versus oxygen partial pressure and stirring rate values are shown in Fig. 17.

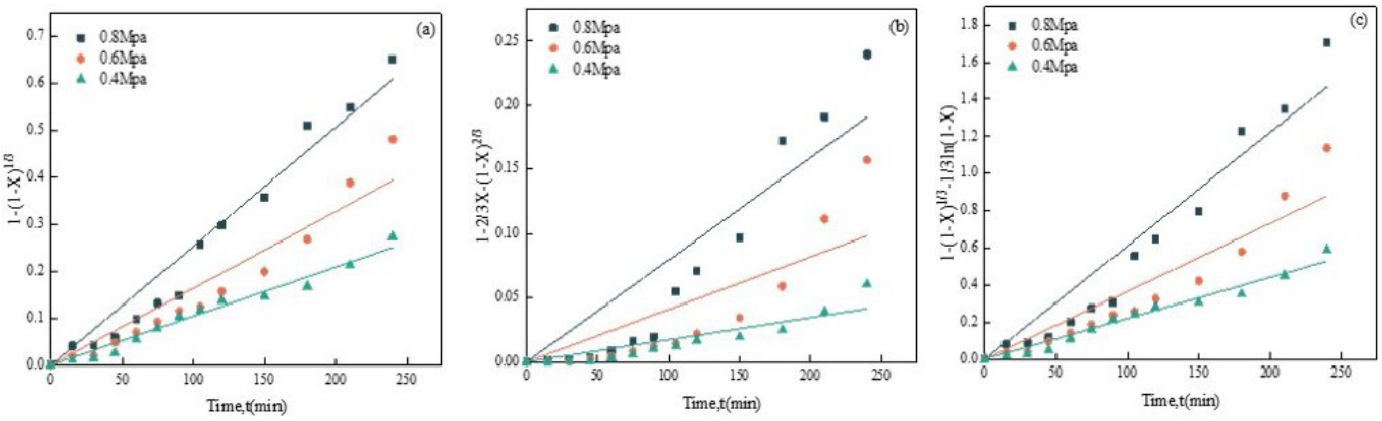

Fig. 15. Fitting curves for the variation of kinetic functions at different oxygen partial pressures (a: $1 - 1(1 - X)^{1/3}$; b: $1 - 2/3X - (1 - X)^{2/3}$; c: $1 - (1 - X)^{1/3} - 1/3\ln(1 - X)$)

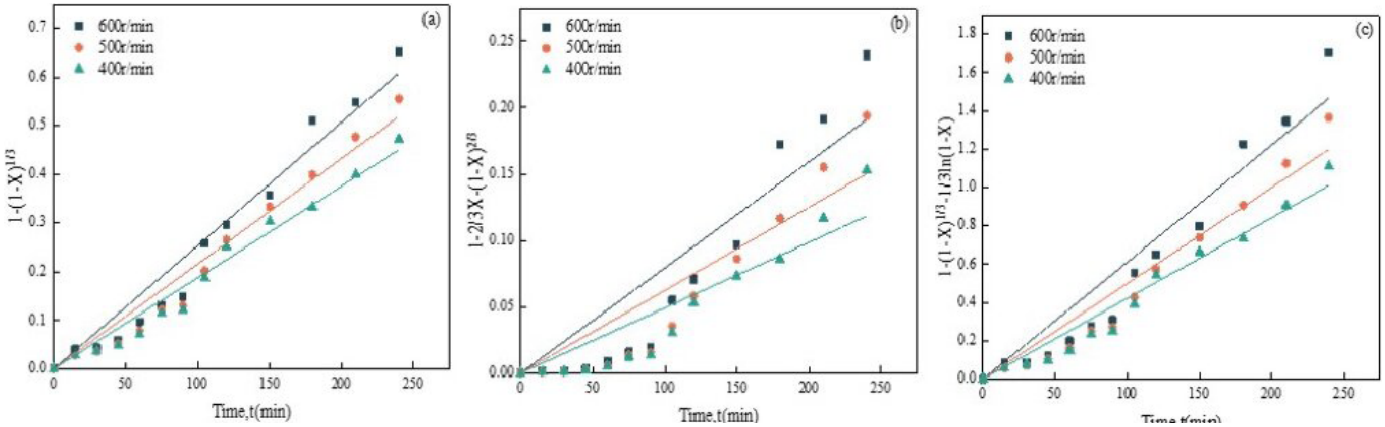

Fig. 16. Fitting curves for the variation of kinetic functions at different stirring rates (a: $1 - 1(1 - X)^{1/3}$; b: $1 - 2/3X - (1 - X)^{2/3}$; c: $1 - (1 - X)^{1/3} - 1/3\ln(1 - X)$)

From the figure, it can be achieved that the reaction order for different oxygen partial pressure is 1.258 and the reaction order for different stirring rates is 0.728.

Substituting the above data into Eq. (7) results in a K_0 value of 0.437, and the macroscopic kinetic equation for leaching copper from CPSSC under oxygen pressure with water as leaching agent can be expressed as:

$$1-\left(1-X\right)^{\frac{1}{3}} = 0.437P_{O_2}^{1.258}w^{0.728}e^{\frac{-5049.7}{T}}t$$

TABLE 4

Parameters of control model at different oxygen partial pressures

Oxygen partial pressure	Chemical reaction control model		Internal diffusion control model		Mixing control model	
	K_r	R^2	K_d	R^2	K_m	R^2
0.8 Mpa	2.530×10^{-3}	0.983	7.961×10^{-4}	0.905	6.110×10^{-3}	0.967
0.6 Mpa	1.640×10^{-3}	0.964	4.110×10^{-4}	0.800	3.660×10^{-3}	0.944
0.4 Mpa	1.050×10^{-3}	0.990	1.740×10^{-4}	0.895	2.210×10^{-3}	0.988

TABLE 5

Parameters of control model at different stirring rates

Stirring rate	Chemical reaction control		Internal diffusion control		Mixing control	
	K_r	R^2	K_d	R^2	K_m	R^2
600 r/min	2.530×10^{-3}	0.983	7.961×10^{-4}	0.905	6.110×10^{-3}	0.967
500 r/min	2.160×10^{-3}	0.986	6.255×10^{-4}	0.902	5.000×10^{-3}	0.975
400 r/min	1.880×10^{-3}	0.989	4.935×10^{-4}	0.914	4.210×10^{-3}	0.983

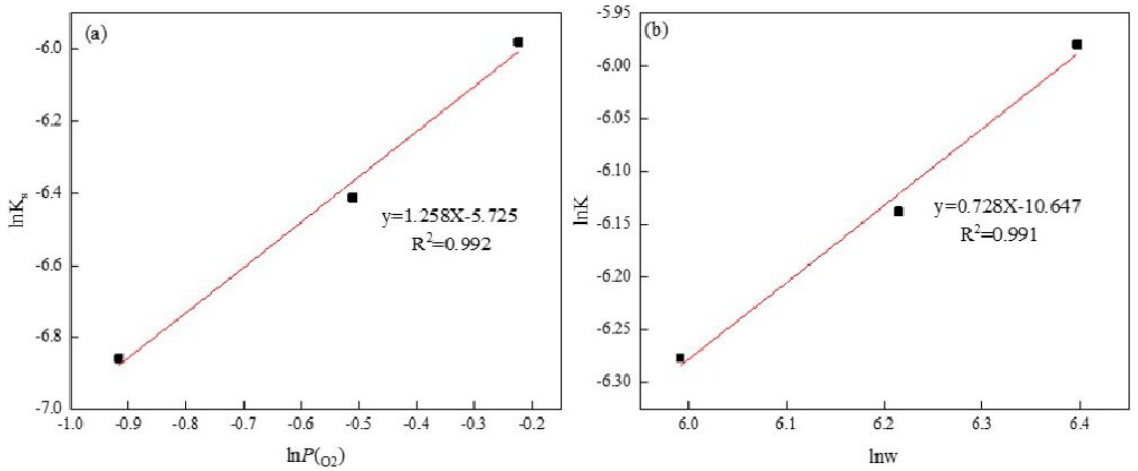

Fig. 17. Relationship between $\ln K_r$ and $\ln P(O_2)$, $\ln W$, respectively

4. Conclusion

(1) By thermal activation pretreatment, more preferable results can be achieved while hydrothermal leaching under oxygen pressure with water is performed on CPSSC. The optimum process conditions for hydrothermal leaching under oxygen pressure of CPSSC after thermal activation pretreatment are as follows: leaching temperature 185°C, oxygen partial pressure 0.6 MPa, liquid to solid rate 12.5:1 and stirring rate 600 r/min. Under the above process conditions, the leaching rate of Cu reached 95.73%.

(2) Combined the structural characterization by XRD and SEM-Mapping, iron oxides and lead sulfate are the main contents in the leached residue obtained under hydrothermal leaching conditions, meaning it can be easy utilized.

(3) The leaching kinetics of copper from CPSSC by hydrothermal leaching under oxygen pressure with water follows chemical reaction control model, which can be expressed as $1-\left(1-X\right)^{\frac{1}{3}} = 0.437 P_{O_2}^{1.258} w^{0.728} e^{\frac{-5049.7}{T}} t$, and the activation energy calculated by Arrhenius equation is 41.98 kJ/mol.

Acknowledgments

The authors express the sincere appreciation to the National Natural Science Foundation of China for the financial support (Project No. 21978122).

REFERENCES

[1] Y. Li, N. Kawashima, J. Li, A.P. Chandra, A.R. Gerson, A Review of the Structure, and Fundamental Mechanisms and Kinetics of the Leaching of Chalcopyrite. Adv. Colloid. Interfac. **197/198**, 1-32 (2013).

[2] Z.J. Huang, J.J. Wang, W. Sun, Y.H. Hu, J. Cao, Z.Y. Gao, Selective Flotation of Chalcopyrite from Pyrite using Diphosphonic Acid as Collector. Miner. Eng. **140**, 105890 (2019).

[3] A. Ghahremaninezhad, D.G. Dixon, E. Asselin, Electrochemical and XPS Analysis of Chalcopyrite ($CuFeS_2$) Dissolution in Sulfuric Acid Solution. Electrochim. Acta **87**, 97-112 (2013).

[4] T.J. Peng, D. Zhou, X.D. Liu, R.L. Yu, T. Jiang, G.H. Gu, M. Chen, G.Z, Qiu, W.M. Zeng, Enrichment of Ferric Iron on Mineral Surface during Bioleaching of Chalcopyrite. T. Nonferr. Metal. Soc. **26**, 544-550 (2016).

[5] J.Y. Wang, L.B. Xie, L.B. Han, X.G. Wang, J.M. Wang, H.B. Zeng, In-Situ Probing of Electrochemical Dissolution and Surface Properties of Chalcopyrite with Implications for the Dissolution Kinetics and Passivation Mechanism. J. Colloid. Interf. Sci. **584**, 103-113 (2021).

[6] Z.Y. Tian, H.D. Li, Q. Wei, W.Q. Qin, C.R. Yang. Effects of Redox Potential on Chalcopyrite Leaching: an Overview. Miner. Eng. **17**, 107135 (2021).

[7] J.X. Hu, G.C. Tian, F.T. Zi, X.Z. Hu, Leaching of Chalcopyrite with Hydrogen Peroxide in 1-Hexyl-3-Methyl-Imidazolium Hydrogen Sulfate Ionic Liquid Aqueous Solution. Hydrometallurgy **169**, 1-8 (2017).

[8] H.R. Watling, Chalcopyrite Hydrometallurgy at Atmospheric Pressure:1. Review of Acidic Sulfate, Sulfate-Chloride and Sulfate-Nitrate Process Options. Hydrometallurgy **140**, 163-180 (2013).

[9] B. Wang, Y.B. Li, S.P. Zhang, L.Q. Luo, Effect of Mechanical Activation on Chalcopyrite Leaching Kinetics. Chin. Min. Mag. **27** (2), 136-140 (2018).

[10] Y.L. Huang, Y.S. Zhang, H.B. Zhao, Y. Zhang, Y. Xiong, L. Zhang, J. Zhou, J. Wang, W. Qin, G. Qiu, Bioleaching of Chalcopyrite-Bornite and Chalcopyrite-Pyrite Mixed Ores in the Presence of Moderately Thermophilic Microorganisms. Int. J. Electrochem. Sc. **12**, 10493-10510 (2017).

[11] T. Tapera, J. Sheean, A.N. Nikolosi, The Effect of Silver on the Acidic Ferric Sulfate Leaching of Primary Copper Sulfides under Recycle Solution Conditions Observed in Heap Leaching. Part 2: Synergistic Additives. Hydrometallurgy **179**, 1-7 (2018).

[12] Y.J. Xian, S.M. Wen, J.S. Deng, J. Liu, Q. Nie, Leaching Chalcopyrite with Sodium Chlorate in Hydrochloric Acid Solution. Canadian Metall. Quart. **52** (2), 133-140 (2012).

[13] S.J. Petrovic, G.D. Bogdanovic, M.M. Antonijevic, Leaching of Chalcopyrite with Hydrogen Peroxide in Hydrochloric Acid Solution. T. Nonferr. Met. Soc. **28**, 1444-1455 (2018).

[14] F. Dakubo, J.C. Baygents, J. Farrell, Peroxodisulfate Assisted Leaching of Chalcopyrite. Hydrometallurgy **121/124**, 68-73 (2012).

[15] A. Al-Zubeidi, D. Godfrey, T. Albrecht, Disentangling Chemical Effects in Ionic- Liquid- Based Cu Leaching from Chalcopyrite. Electroanal. Chem. **819**, 130-135 (2018).

[16] X.M. Hua, Y.F. Zhang, Q. Xu, X. Lu, H. Cheng, X. Zou, Q. Song, Z. Ning, Interfacial Reactions of Chalcopyrite in Ammonia-Ammonium Chloride Solution. T. Nonferr. Met. Soc. **116**, 509-516 (2018).

[17] J. Cháidez, J. Parga, J. Valenzuela, R. Carrillo, I. Almaguer, Leaching Chalcopyrite Concentrate with Oxygen and Sulfuric Acid using a Low-Pressure Reaction. Metals **9**, 189 (2019).

[18] P. Prameena, G. Anbalagan, S. Gunasekaran, G.R. Ramkumaar, B. Gowtham, Structural, Optical, Electron Paramagnetic, Thermal and Dielectric Characterization of Chalcopyrite. Spectrochim. Acta A **122**, 348-355 (2014).

[19] J.J. Xi, G.X. Ji, Y.L. Liao, Q.F. Liu, Y. Wu, Study on Selective Leaching of Copper and Simultaneous Precipitation of Iron in Polymetallic Complex Chalcopyrite by Hydrothermal Leaching under Oxygen Pressure. Metall. Mater. Trans. B **54**, 2575-2590 (2023).

[20] X.H. Zheng, W.G. Lv, H.B. Cao, N. Cai, J. Chen, Q.C. Li, F. Kang, Z. Sun, Leaching of Valuable Metals from Nickel Sulfide Ores by Mechanical Activation. Chin. J. Process Eng. **21** (9), 1064-1073 (2021).

[21] T.G. Wen, Y.L Zhao., Q.L. Ma, Q. Xiao, T. Zhang, J. Chen, S. Song, Microwave Improving Copper Extraction from Chalcopyrite through Modifying the Surface Structure. J. Mater. Res. Technol. **9**, 263-270 (2020).

[22] S.H. Sun, F.S. Pan, Y.B. Xie, H. Cao, Y. Zhang. Chemical Oxidation Strengthening Cleaner Production of Hydrometallurgy:

Progress and Prospect. Chin. J. Process Eng. **22** (02), 145-161 (2022).

[23] J.X Wang, F. Faraji, A. Ghahreman, Effect of Ultrasound on the Oxidative Copper Leaching from Chalcopyrite in Acidic Ferric Sulfate Media. Minerals **10** (7), 1-17 (2020).

[24] M. Al-Harahsheh, S. Kingman, N. Hankins, C. Somerfield, S. Bradshaw, W. Louw, The Influence of Microwave on the Leaching Kinetics of Chalcopyrite. Miner. Eng. **18**, 1259-1268 (2005).

[25] Beijing General Research Institute of Mining and Metallurgy, Ores and Non-Ferrous Metals Analysis Manual, 1990 Metallurgical Industry Press, Beijing.

[26] Y.L. Bai, W. Wang, K.W. Dong, F. Xie, D. Lu, Y. Chang, K. Jiang, Effect of Microwave Pretreatment on Chalcopyrite Dissolution in Acid Solution. J. Mater. Res. Technol. **16**, 471-481 (2022).

[27] V.K. Berry, L.E. Murr, J.B. Hiskey, Galvanic Interaction Between Chalcopyrite and Pyrite During Bacterial Leaching of Low- Grade Waste. Hydrometallurgy **3**, 309-326 (1978).

[28] M.K. Tanaydin, Z.B. Tanayadin, N. Demirkiran, Optimization of Process Parameters and Kinetic Modeling for Leaching of Copper from Oxidized Copper Ore in Nitric Acid Solutions. T. Nonferr. Met. Soc. **32**, 1301-1313 (2022).

[29] B.S. Han, B. Altansukh, K. Haga, Y. Takasaki, A. Shibayama, Leaching and Kinetic Study on Pressure Oxidation of Chalcopyrite in H_2SO_4 Solution and the Effect of Pyrite on Chalcopyrite Leaching. J. Sust. Metall. **3**, 528-542 (2017).

[30] X.W. Yang, A.P. He, B.Z. Yan, H. Hu, Manual for calculation of thermodynamic data of high temperature aqueous solution, 1983 Metallurgical Industry Press, Beijing.

[31] O. Levenspiel, Chemical Reaction Engineering (3rd ed), 1999 John Wiley & Sons, New York.

[32] C.F. Dichinson, G.R. Heal, Solid-Liquid Diffusion-Controlled Rate Equations. Thermochim. Acta **340/341**, 89-103 (1999).

[33] H.H. Wang, G.Q. Li, D. Zhao, J.H. Ma, J. Yang, Dephosphorization of High Phosphorus Oolitic Hematite by Acid Leaching and the Leaching Kinetics. Hydrometallurgy **171**, 61-68 (2017).

[34] M. Ashrsf, I.Z. Zafar, T.M. Ansari, Selective Leaching Kinetics and Upgrading of Low-Grade Calcareous Phosphate Rock in Succinic Acid. Hydrometallurgy **80** (4), 286-292 (2005).

[35] G. Ji, Y. Liao, J. Xi, Q.F. Liu, Y. Wu, H.F. Ma, J.L. Li, Behavior and Kinetics of Copper During Oxygen Pressure Leaching of Complex Chalcopyrite without Acid. J. Sust. Metall. **9**, 350-362 (2023).

[36] F.K. Urakaev, V.V. Boldyrev, Mechanism and Kinetics of Mechanochemical Processes in Comminuting Devices: 1. Theory. Powder Technol. **107** (1/2), 93-107 (2000).

[37] T.A. Haug, Dissolution and Carbonation of Mechanically Activated Olivine – Investigating CO_2 Sequestration Possibilities. PhD thesis, Norwegian University of Science and Technology, 2010.

[38] W.L. Wang, K. Sun, Q.X. Huang, J.H. Yan, Effect of Inorganic Ash on Pyrolysis Characteristics of Organic Matter of Biogas Residue from Food Waste. Journal of Zhejiang University (Engineering Science) **55** (9), 1652-1659 (2021).

[39] M. Li, X.W. Zhang, Z.G. Liu, Y. Hu, M. Wang, J. Liu, J. Yang, Kinetics of Leaching Fluoride from Mixed Rare Earth Concentrate with Hydrochloric Acid and Aluminum Chloride. Hydrometallurgy **140**, 71-76 (2013).

[40] J. Tian, J.Q. Yin, R. Chi, G. Rao, M. Jiang, K. Ouyang, Kinetics on Leaching Rare Earth from the Weathered Crust Elution-Deposited Ores with Ammonium Sulfate Solution. Hydrometallurgy **101**, 166-170 (2010).